CREEP AND MICROSTRUCTURAL EVOLUTION AT HIGH TEMPERATURE OF LIQUID-PHASE-SINTERED SILICON CARBIDE

Juan J. Meléndez-Martínez[1, *, a], Miguel Castillo-Rodríguez[1], Angel L. Ortiz[2,&], Fernando Guiberteau[2] and Arturo Domínguez-Rodríguez[1, §]

Abstract

The compressive creep characteristics at 1625 ºC of liquid-phase-sintered silicon carbide ceramics containing 5 wt% and 15 wt% of crystalline $Y_3Al_5O_{12}$ (YAG) as secondary phase were studied. In the two cases, strains between 10% and 15% were reached without failure. The creep behaviour was characterized by a stress exponent $n \approx 2$, and the proportion of secondary phase was related to the creep resistance of the materials. The microstructural evolution during creep consisted firstly in the redistribution of the secondary phase, probably as a consequence of its viscous flow at the creep conditions, and secondly an extensive nucleation and growth of cavities which was more important for the highest YAG content. The latter reflects the carbothermal reduction that the secondary phase undergoes during creep.

Keywords: Silicon carbide, creep behaviour, microstructure.

[1] Departamento de Física de la Materia Condensada. Universidad de Sevilla. P. O. 1045. 41081, Sevilla (Spain).

[*] Permanent address: Departamento de Física. Universidad de Extremadura. Avda. de Elvas, s/n. 06071, Badajoz (Spain).

[2] Departamento de Electrónica e Ingeniería Electromecánica. Universidad de Extremadura. Avda. de Elvas, s/n. 06071, Badajoz (Spain).

[a] Corresponding author.

[&] Member, American Ceramic Society.

[§] Fellow, American Ceramic Society.

1. INTRODUCTION

During the last decade, non-oxide ceramics have taken on an unquestionably important position. Silicon nitride is a good example of this[1]. But silicon carbide (SiC) has also recently been shown to exhibit exceptional features for structural applications. The set of properties of SiC includes great hardness and strength with moderate toughness[2], high resistance against aggressive chemical attack[3], high resistance to oxidation and wear[4,5], high thermal conductivity and thermal-shock resistance[6], and excellent strength retention at high temperatures[7]. These make SiC-based materials suitable for such industrial applications as muffle furnace linings, kiln parts, and especially as parts of high-temperature heat exchangers[8].

The densification of SiC ceramics is generally achieved by liquid-phase sintering with the help of oxide additives[2]. The additives promote the formation of a liquid phase at relatively low temperatures (1750 to 2000 ºC), and densification occurs by liquid rearrangement and solution-precipitation. After cooling, the liquid remains as a secondary phase, located at multigrain junctions and as intergranular film, which affects the mechanical properties of the resulting material. For instance, liquid-phase-sintered (LPS) SiC ceramics processed with mixtures of AlN, Y_2O_3, and RE_2O_3 (RE = rare earth) as sintering aids have been shown to possess excellent fracture toughness, creep resistance, and strength at high temperatures when compared with solid-state-sintered (SSS) SiC ceramics[7,9]. One of the most widely studied additive systems is Y_2O_3 - Al_2O_3, especially when these components are chosen in the ratio 3:5 to form yttrium-aluminum garnet (YAG, $Y_3Al_5O_{12}$)[10,11]: the presence of crystalline YAG has been demonstrated to improve the fracture toughness at room temperature of LPS SiC[2].

The high-temperature compressive creep of SiC has been the interest of several works before[12-24], although it has yet to be systematically studied. In particular, to the best of the authors' knowledge, the correlation between creep behaviour and microstructural evolution in LPS SiC containing crystalline YAG as secondary phase has only been studied once before, showing the effect of sintering time[24]. As a complement to that study, the present work was aimed at shedding light on that correlation by studying two LPS SiC ceramics containing different proportion of crystalline YAG, both processed under the same heat-treatment conditions. In particular, it will be shown that, even though their microstructure is greatly degraded during creep due to the evolution of the secondary phase, the materials exhibit interesting characteristics for high temperature applications.

2. EXPERIMENTAL PROCEDURE

The starting powders were commercial, ultrafine powders of α-SiC (UF-15, H. C. Starck, Berlin, Goslar, Germany), Al_2O_3 (AKP-30, Sumitomo chemical Company, New York, NY), and Y_2O_3 (Fine Grade, H. C. Starck, Berlin, Goslar, Germany). These powders were combined in the proportions given in table I, resulting in α-SiC composites with 5 wt% and 15 wt% $Y_3Al_5O_{12}$ (YAG) (that is, 3.6 vol.% and 11.1 vol.%, respectively). The powder mixtures were then ball-milled in ethanol for 24 h using zirconia balls media and polyethylene bottles. The resulting slurries were subsequently dried on hot-plates while being stirred. The dried powders were next crushed and sieved to remove the hard agglomerates. Compacts were made from each of the powder batches by uniaxial compaction in graphite dies at 50 MPa, followed by isostatic compaction at 350 MPa in water within latex globes. The pellets were then placed in graphite crucibles containing coarse Al_2O_3 and SiC powders (used as powder beds), and subsequently pressureless sintered in a graphite furnace. The sintering conditions were:

peak temperature of 1950 ºC, heating and cooling rates of 600 ºC·h^{-1}, hold time at peak temperature of 2 h, and flowing argon atmosphere. The sintered materials were ground down 1 mm to remove the adhered powder bed layer, and were then rinsed clean with acetone and ethanol. The indentation hardness (H_V) and toughness (K_{IC}) of the two LPS SiC ceramics at room-temperature were measured by Vickers tests at 98 N load (ten separate indentations per each material), and the obtained values are given in table I; elastic modulus (E) values determined using Hertzian indentations were used in the K_{IC} calculations.

The mechanical behaviour of the processed materials was investigated by uniaxial compression creep tests on samples cut and ground as parallelepipeds of approximate dimensions 5 × 3 × 3 mm^3. The tests were performed on a prototype dead-load creep machine fitted with SiC push-rods and a hemispherical furnace. The temperature was continuously monitored throughout the test (within ± 1 ºC) with a W-10 % Re / W-26 % Re thermocouple placed near the sample. The instantaneous length of the sample was recorded (within ± 2 μm) by an LVDT located outside the furnace. Additional details of the experimental device have been given elsewhere[25]. The tests were carried out at 1625 ºC, at stresses ranging between 40 MPa and 90 MPa, approximately, and were stopped without failure of the samples. To avoid the oxidation of the samples, all the tests were performed in a controlled argon atmosphere.

The microstructures of the undeformed and crept samples were examined by scanning electron microscopy (Model XL30, Philips Research Laboratories, Eindhoven, The Netherlands) using both secondary (SE) and back-scattered electrons (BSE). For the undeformed samples, the observation surfaces were chosen arbitrarily; for crept samples, they were chosen parallel to the compression axis. In all cases, the observation surfaces were first ground and then polished with diamond paste to 3 μm finish.

Subsequently, they were plasma-etched using a mixture of CF_4 and O_2 in the ratio 1:6 for 135 min to reveal the grain boundaries, and then gold–coated. The grain diameter (d; defined as $d = (4\times\text{Area}/\pi)^{1/2}$), and form factor (F; defined as $F = 4\pi\times\text{Area}/(\text{Perimeter})^2$) were measured from SEM micrographs using a semi-automatic image analyzer (Kontron MOP 30) on no less than 300 grains.

3. RESULTS

3.1. Microstructural characterization of the as-sintered samples

Figure 1a shows a typical SEM micrograph of SiC-5YAG. After sintering, this material was fully dense ($\rho = 3.26$ g·cm^{-3}). The microstructure consists of equiaxed SiC grains (dark phase), among which the secondary phase (crystalline YAG[26]), in bright contrast, is homogeneously distributed as pockets located at triple points of the grain structure. An amorphous film at the grain boundaries is likely to be present[27], although it was not observed by SEM. The characteristic core-rim structure of the SiC grains, resulting from grain growth during sintering[28], is clearly observed. The grain size (taken as the planar equivalent diameter) and form factor of this material were 0.7 ± 0.3 μm and 0.95 ± 0.05, respectively.

The microstructure of SiC-15YAG is similar to that described above, as shown clearly in Fig. 1b; in particular, about the same grain sizes and form factors were measured (cf. table I). The main differences result from the absolute density ($\rho = 3.36$ g·cm^{-3} for SiC-15YAG, fully dense) and the distribution of the secondary phase, which is somewhat less homogeneous than in the material containing 5 wt % YAG.

3.2. Mechanical behaviour

The creep curves (log $\dot{\varepsilon}$ vs. ε) at 1625 ºC for SiC-5YAG and SiC-15YAG are shown in figs. 2a and 2b. For comparison purposes, the applied stress and the strain

attained at each stage of the creep tests were similar for the two materials. The creep curves reveal some interesting properties. In all cases, the steady-state regime is reached almost immediately after loading; significant transient states appear mostly at the first loading stage. At each stress stage, once the steady-state has been reached, the strain that the materials are able to undergo can be high (see, for instance, the first stage in fig. 2b, with $\varepsilon = 6.9\%$). The total strain (without failure) is higher than 15% for SiC-15YAG, and about 10% for SiC-5YAG. These values compare well with previous results in LPS SiC containing Y_2O_3 and Al_2O_3 as sintering aids[12,29] and also for some SSS SiC[14,17]. As will be clear below, it is also important to note the duration of the tests: this was about 120 h for SiC-5YAG and more than 150 h for SiC-15YAG.

The observed range of strain rates lies between about 10^{-7} s^{-1} (SiC-5YAG under 49.4 MPa) and about $6 \cdot 10^{-7}$ s^{-1} (SiC-15YAG under 90.6 MPa), These strain rates are also in good agreement with previously reported results in similar systems[12,24]. In addition, the materials studied here are significantly more creep resistant than some SSS SiC[14,17] and superplastic LPS SiC[30]. Figure 3 compares the strain rate versus stress logarithmic plot at the creep temperature for the two materials. At a given stress, the strain rate increases with the YAG content: the higher the proportion of secondary phase, the lower the creep resistance of the material. No evidence for accelerated creep, generally associated with damage development, was observed in any case. One can hence state that SiC-5YAG and SiC-15YAG exhibit reasonably good ductility and creep resistance at high temperature. The experimental results therefore demonstrate that the applicability of YAG-sintered SiC as a structural material is not restricted to temperatures below the 1345 ºC eutectic temperature, as has been pointed out elsewhere[4].

The creep results are analyzed in terms of the classical power-law creep equation:

$$\dot{\varepsilon} \propto \sigma^n \quad (1)$$

where $\dot{\varepsilon}$ is the steady-state strain rate, σ is the applied stress, and n is the stress exponent for creep, which can be calculated at each stress change[31]. The measured stress exponents for SiC-5YAG and SiC-15YAG are included in figs. 2. An average value $n \approx 2$ was obtained for both materials under the present experimental conditions (see Fig. 3), in good agreement with previously reported values for SiC[12,17,20,24].

3.3. Microstructure of the deformed materials

Figures 4a and 4b show typical SEM micrographs of SiC-5YAG and SiC-15YAG after the creep tests, respectively. A comparison of these micrographs with the corresponding ones in Figs 1a and 1b reveals that during creep, no dynamic grain growth took place, and the grains maintained their mean size and their equiaxed shape. However, creep affected the microstructure of the materials in two principal ways. Firstly, it was evident that the secondary phase is expelled from some grain boundaries (presumably those subjected to compressive stresses), and rearranged in others. Figures 4a and 4b show this for SiC-5YAG and SiC-15YAG, respectively.

The second main microstructural evolution consisted in the extensive growth and coalescence of large, isolated cavities. Figures 5 and 6 ((a) close to the center of the samples, to (c) near the surface) show this feature for SiC-5YAG and SiC-15YAG, respectively. The surface density (i.e., number of cavities per unit area) and the size of the cavities increase rapidly from the center to the surface of each sample. The cavities show a harsh elongation in a plane perpendicular to the compression axis: this effect becomes even more pronounced as one approaches the surfaces. Instead, the cavities

that form in the absence of applied load are equiaxed and smaller, as seen in Fig. 7 for specimens placed inside the creep machine during the tests but not loaded. It was also observed that cavitation was significantly more important in SiC-15YAG than in SiC-5YAG. Similar results have been described elsewhere[24] for an LPS SiC containing 10 wt % YAG, although the cavitation was much less severe than that observed here.

4. Discussion

To ascribe the measured stress exponents to microscopic deformation mechanisms requires a prior detailed analysis of the microstructural evolution. This can be done in terms of a series of concurrent kinetic processes accompanying creep. Let us first consider the redistribution of the secondary phase mentioned above. One can argue in terms of the well-known viscous flow creep models[32,33], since the viscosity of the secondary phase at the testing temperature is low enough to allow its squeezing from the grain boundaries under compression. According to this mechanism, the secondary phase is squeezed out from grain boundaries under compression and accumulates in multigrain pockets that are under only slight compressive stresses. Consequently, the flow of the secondary phase can explain the appearance of large pockets of secondary phase and relatively extensive regions of interlocked grains depleted of it. In addition, if viscous flow of the secondary phase proceeds for a relatively long time (i.e., if high final strains are attained), then one would expect the aforementioned agglomerations to locate preferentially near the outer surfaces of the samples, where they would be larger in size. Therefore, viscous flow is compatible with some of the observed microstructural features, although it cannot alone explain the observed severe cavitation. In addition, it is also incompatible with the creep characteristics cited above: due to its inherently transient nature, high strains in the steady-state cannot be attained by this mechanism.

Second, YAG-containing LPS SiC may undergo chemical transformations at the high temperatures required for creep. For instance, passive oxidation of SiC may occur[34,35]. Oxidation of SiC is expected to give rise to a narrow layer of oxide at the surface of the samples: this surface was not clearly observed here because of the extensive damage. For the present work, the most important chemical change consists of the reactions between YAG and SiC at the creep temperatures, as also was observed in the previous work[24]. It has been reported that substantial weight loss may occur during sintering of Y_2O_3 - Al_2O_3 - SiC containing free Al_2O_3. This has been attributed to the reaction between the free Al_2O_3 and the SiC, resulting in the formation of volatile species. According to the literature, the most probable reaction is[11]:

$$SiC\ (s) + Al_2O_3\ (s) \leftrightarrow Al_2O\ (g) + SiO\ (g) + CO\ (g) \qquad (2)$$

Other reactions between SiC (s) and Al_2O_3 (s) to form Al_2OC (g) and/or Al_4O_4C (g) have also been reported elsewhere[36]. A reaction similar to (2) involving Y_2O_3 is also likely to occur.

In addition, yttrium aluminates [$Y_3Al_5O_{12}$ (YAG), $YAlO_3$ (YAP), $Y_4Al_2O_9$ (YAM)] have been shown to decompose in presence of SiC at high temperatures, even in the absence of free Al_2O_3. Indeed, Mah and co-workers[10] showed that YAG was highly stable at up to 1650 ºC in air and under vacuum, but undergoes severe decomposition at temperatures as low as 1500 ºC under vacuum in the presence of SiC. The decomposition of YAG was accompanied by the formation of aluminium-containing gaseous species, which are most likely to escape from the specimen. The authors explained this effect as being associated with the carbothermal reduction of YAG, which proceeds via the following decomposition reaction:

$$Y_3Al_5O_{12}\ (s) + 4CO\ (g) \leftrightarrow 3YAlO_3 + Al_2OC\ (g) + 3CO_2\ (g) \qquad (3)$$

being the source of gaseous CO the active oxidation of SiC under low oxygen partial pressures:

$$SiC\ (s) + O_2\ (g) \leftrightarrow SiO\ (g) + CO\ (g) \qquad (4)$$

Grande and co-workers have also identified this process at higher temperatures[11].

Now consider the aforementioned agglomerations of crystalline YAG generated by viscous flow. The formation of volatile species accompanying their carbothermal reduction may then well be at the origin of the observed extensive nucleation and spectacular growth of cavities. The same carbothermal reduction of YAG may explain why cavitation becomes even more important as one approaches the outer surfaces of the samples (since, as mentioned above, YAG tends to flow outward as creep proceeds). This scenario is also consistent with the fact that cavitation is much more severe in SiC-15YAG: this material contains more secondary phase, and in addition was subjected to high temperatures over a much longer time.

The validity of the above argumentation was evaluated by EDX analysis. Compared in figs. 8a and 8b are the EDX spectra of SiC-5YAG and SiC-15YAG before and after the creep tests, respectively. As seen in Fig 8, there is no discernible Al peak in the EDX spectra of the two crept specimens, which is direct evidence of loss of Al during the creep tests. Thus, the EDX analysis is consistent with the existence of carbothermal reduction of YAG at the creep conditions. Note that, as a consequence of the aforementioned reactions, the composition of the secondary phase changes as creep proceeds. Consequently, the white-contrast phases in figs. 4 are expected to be well different than those shown in figs. 1.

Most of the microstructural characteristics described above may be explained in terms of a viscous flow plus carbothermal reduction of YAG coupled process. At the creep temperature, viscous flow makes SiC grain boundaries under compression come

into contact as well as agglomerating the YAG squeezed out from these grain boundaries into large pockets. The size and density of these pockets is expected to grow as one approaches the surfaces of the samples. Simultaneously, the YAG in the pockets undergoes carbothermal reduction, which gives rise to several volatile species and nucleates cavities in the large pockets formed by viscous flow. Finally, these cavities are deformed in a plane perpendicular to the compression axes because of the action of the applied stress.

From the analysis of the complex kinetic processes which are involved in the creep of the materials, the identification of microscopic deformation mechanisms is formidably difficult. Viscous flow cannot be responsible for the creep behaviour, due to its transient nature. Instead, grain boundary sliding, consistent with the measured stress exponents and with the lack of either dynamic growth or change of shape of the grains, is likely to be the active mechanism. In addition, the growth and change of shape of the cavities may also contribute to both the strain and the strain rate. Finally, dislocation glide and climb have also been identified by TEM during creep of LPS SiC[12,19,22,24], although such TEM observations were not performed in the present study. Thus, it is reasonable to think that the creep behaviour of these materials cannot be explained by the classical scheme of deformation mechanism plus accommodation (rate-controlling) mechanism. Instead, the observed steady-state creep seems to result from the contributions of a set of simultaneous and concurrent processes (grain boundary sliding + viscous flow of the secondary phase + chemical transformation of YAG + formation and growth of cavities + (likely) dislocation activity).

In spite of the obvious difficulties associated with the identification of creep mechanisms, and from the viewpoint of the possible structural applications of these materials, it should be remarked that the materials exhibit relatively good creep

characteristics (especially creep resistance and ductility) without evidence of failure. The suitability of YAG-containing SiC for high-temperature applications is thus demonstrated.

5. CONCLUSIONS

The compressive creep characteristics at 1625 ºC and the microstructural evolution during creep of two LPS SiC polycrystals containing 5 wt% and 15 wt% crystalline YAG as secondary phase were studied. Steady-state creep extended to strains up to about 15 % without evidence of failure: stress exponents close to 2 were measured. The microstructural evolution during creep consisted, first, of the redistribution of the secondary phase and, second, of the extensive nucleation and growth of large cavities. This evolution was explained in terms of a coupled viscous flow + carbothermal reduction of YAG process. Finally, steady-state creep results from the contribution of a set of simultaneous processes instead of from the classical scheme of deformation mechanism + accommodation mechanism. It was noteworthy that, in spite of the degradation of the microstructure, the materials exhibited good creep properties (ductility and creep resistance), which compare well with results reported for other SiC ceramics.

Acknowledgements

This work was supported by the Ministerio de Ciencia y Tecnología (Government of Spain) and the Fondo Europeo de Desarrollo Regional (FEDER) under grant Nos. CICYT MAT 2004-05971 and UNEX00-23-013. JJMM thanks the Consejería de Infraestructuras y Desarrollo Tecnológico (Junta de Extremadura) for supporting his stays at the University of Seville. Fruitful discussions with Prof A. Muñoz-Bernabé of the University of Seville are gratefully acknowledged.

References

[1] J. J. Meléndez-Martínez and A. Domínguez-Rodríguez, "Creep of silicon nitride", *Prog. Mat. Sci.*, **49** [1] 19-107 (2004).

[2] N. P. Padture, "In-situ toughened silicon carbide", *J. Am. Ceram. Soc.*, **77** [2] 519-523 (1994).

[3] K. A. Schwetz, "Silicon carbide-based hard materials", pp. 683-740 in Handbook of Ceramic Hard Materials. Edited by R. Riedel. Wiley-VCH, Weinheim, Germany, 2000.

[4] R. P. Jensen, W. E. Luecke, N. P. Padture and S. M. Wiederhorn, "High-temperature properties of liquid-phase-sintered α-SiC", *Mat. Sci. Eng.*, **A282** [1-2] 109-114 (2000).

[5] V. S. R. Murthy, H. Kobayashi, N. Tamari, S. Tsurekawa, T. Watanabe and K. Kato, "Effect of doping elements on the friction and wear properties of SiC in unlubricated sliding condition", *Wear*, **257** [1-2] 89-96 (2004).

[6] L. S. Sigl, "Thermal conductivity of liquid-phase-sintered silicon carbide", *J. Eur. Ceram. Soc.* **23** [7] 1115-1122 (2003).

[7] Y.-W. Kim, M. Mitomo and T. Nishimura, "High-temperature strength of liquid-phase-sintered SiC with AlN and RE_2O_3 (RE = Y, Yb)", *J. Am. Ceram. Soc.* **85** [4] 1007-1009 (2002).

[8] S. J. Dapkunas, "Ceramic heat-exchangers", *Am. Ceram. Soc. Bull.*, **67** [2] 388-391 (1988).

[9] Y.-W. Kim, M. Mitomo and T. Nishimura, "Heat-resistant silicon carbide with aluminum nitride and erbium oxide", *J. Am. Ceram. Soc.*, **84** [9] 2060-2064 (2001).

[10] T.-I. Mah, K. A. Keller, S. Sambasivan and R. J. Kerans, "High-temperature environmental stability of the compounds in the Al_2O_3-Y_2O_3 system", *J. Am. Ceram. Soc.*, **80** [4] 874-878 (1997).

[11] T. Grande, H. Sommerset, E. Hagen, K. Wiik and M. A. Einarsrud, "Effect of weight loss on liquid-phase-sintered silicon carbide", *J. Am. Ceram. Soc.*, **80** [4] 1047-1052 (2004).

[12] A. Gallardo-López, A. Muñoz, J. Martínez-Fernández and A. Domínguez-Rodríguez, "High-temperature compressive creep of liquid-phase-sintered silicon carbide", *Acta Mater.*, **47** [7] 2185-2195 (1999).

[13] S. Honda, T. Nagano, K. Kaneko and H. Kodama, "Compressive deformation behavior of Al-doped β-SiC at elevated temperature", *J. Eur. Ceram. Soc.*, **22** [6] 979-985 (2002).

[14] Y. Shinoda, M. Yoshida, T. Akatsu and F. Wakai, "Effect of amount of boron doping on compression deformation of fine-grained silicon carbide at elevated temperature", *J. Am. Ceram. Soc.*, **87** [8] 1525-1529 (2004).

[15] S. M. Wiederhorn, B. J. Hockey and J. D. French, "Mechanisms of deformation of silicon nitride and silicon carbide at high temperatures", *J. Eur. Ceram. Soc.*, **19** [13-14] 2273-2284 (1999).

[16] M. L. Duval-Riviere, C. Carry and J. Vicens, "Microstructural study of deformation mechanisms in polycrystalline α-SiC deformed at high temperature", *Phys. Status Solidi*, **155** 6-82 (1996).

[17] Y. Shinoda, M. Yoshida, T. Akatsu and F. Wakai, "Compression deformation mechanism of silicon carbide: I, fine-grained boron- and carbon-doped β-silicon carbide fabricated by hot isostatic pressing", *J. Am. Ceram. Soc.*, **87** [10] 1919-1926 (2004).

[18] A. Djemel, J. Cadoz and J. Philibert, "Deformation of polycrystalline α-SiC", pp. 381-394 in Creep and Fracture of Engineering Materials and Structures. Edited by B. Wilshire and D. R. J. Owen. Pineridge Press, Swansea, United Kingdom, 1981.

[19] J. E. Lane, C. H. Carter Jr. and R. F. Davis, "Kinetics and mechanisms of high-temperature creep in silicon carbide: III, sintered α-silicon carbide", *J. Am. Ceram. Soc.*, **71** [4] 281-295 (1981).

[20] H. Tanaka and Y. Inomata, "Diffusional creep in sintered silicon carbide", *J. Jap. Ceram. Soc.*, **93** [1] 45-50 (1985).

[21] G. Grathwohl, T. H. Reets and F. Thummler, "Creep of hot-pressed and sintered SiC with different sintering additives", *Sci. Ceram.*, **11** 425-431 (1981).

[22] R. D. Nixon and R. F. Davis, "Diffusion accommodated grain boundary sliding and dislocation glide in the creep of sintered alpha silicon carbide", *J. Am. Ceram. Soc.*, **75** [7] 1786-1795 (1992).

[23] Z. C. Jou A. V. Virkar and R. A. Cutler, "High temperature creep of SiC densified using a transient liquid phase", *J. Mater. Res.*, **6** [9], 1945-1949 (1991).

[24] M. Castillo-Rodríguez, A. Muñoz and A. Domínguez-Rodríguez, "Correlation between microstructure and creep behavior in liquid-phase-sintered α-silicon carbide", *J. Am. Ceram. Soc.*, in press.

[25] J. J. Meléndez-Martínez, D. Gómez-García, M. Jiménez-Melendo and A. Domínguez-Rodríguez, "Creep mechanism of gas-pressure-sintered silicon nitride polycrystals I. Macroscopic and microscopic experimental study", *Phil. Mag.* **A84** [31] 3375-3386 (2004).

[26] A. L. Ortiz, F. L. Cumbrera, F. Sánchez-Bajo, F. Guiberteau, H. Xu and N. P. Padture, "Quantitative phase-composition analysis of liquid-phase-sintered silicon carbide using the Rietveld method", *J. Am. Ceram. Soc.*, **83** [9] 2282-2286 (2000).

[27] T. Nagano, H. Gu, G. D. Zhan and M. Mitomo, "Effect of atmosphere on superplastic deformation behavior in nanocrystalline liquid-phase-sintered silicon carbide with Al_2O_3-Y_2O_3 additions", *J. Mater. Sci*., **37** 4419-4424 (2002).

[28] L. S. Sigl and H.-J. Kleebe, "Core/rim structure of liquid-phase-sintered silicon carbide", *J. Am. Ceram. Soc.*, **76** 773-776 (1993).

[29] M. Castillo-Rodríguez, A. Muñoz and A. Domínguez-Rodríguez, "Effect of atmosphere and sintering time on the microstructure and mechanical properties at high temperatures of α-SiC sintered with liquid phase Y_2O_3-Al_2O_3", *J. Eur. Ceram. Soc*, in press.

[30] T. Nagano, K. Kaneko, G.-D. Zhan, M. Mitomo and Y.-W. Kim, "Superplastic behavior of liquid-phase sintered β-SiC prepared with oxynitride glasses in an N_2 atmosphere", *J. Eur. Ceram. Soc.*, **22** [2] 263-270 (2002).

[31] D. Gómez-García, J. Martínez-Fernández, A. Domínguez-Rodríguez. P. Eveno and J. Castaing, "Deformation mechanisms for high-temperature creep of high yttria content stabilized zirconia single crystals", *Acta mater.*, **44** [3] 991-999 (1996).

[32] J. R. Dryden, D. Kucerovsky and D. S. Wilkinson, "Creep deformation due to a viscous grain boundary phase", *Acta metall.*, **37** [7] 2007-2015 (1989).

[33] M. M. Chadwick, D. S. Wilkinson and J. R. Dryden, "Creep due to a non-Newtonian grain boundary phase", *J. Am. Ceram. Soc.*, **79** [9] 2327-2334 (1992).

[34] J. W. Hinze and H. C. Graham, "The active oxidation of Si and SiC in the viscous glass-flow regime", *J. Electrochem. Soc.*, **12** [7] 1066-1073 (1976).

[35] M. Balat, G. Flamant, G. Male and G. Pichelin, "Active to passive transition in the oxidation of silicon carbide at high temperature and low pressure in molecular and atomic oxygen", *J. Mater. Sci.*, **27** 697-703 (1992).

[36] A. Gadalla, M. Elmasry, P. Kongkachuichay: "High temperature reactions within SiC-Al_2O_3 composites", *J. Mater. Res.* **7** [9] 2585-2592 (1992).

Figure captions

Figure 1. SEM micrographs of as-processed A) SiC-5YAG and B) SiC-15YAG showing the grain morphology and phases present.

Figure 2. Creep curve at 1625 ºC for A) SiC-5YAG (stresses between 49 and 91 MPa up to about 10 % of strain) and B) SiC-15YAG (stresses between 43 and 81 MPa up to about 16 % of strain). The values of the stress exponent obtained from each stress change are shown.

Figure 3. Strain rate versus stress logarithmic plot for SiC-5YAG and SiC-15YAG under the experimental conditions used in this study. The average stress exponent obtained by lineal fit is shown for each case.

Figure 4. Grain morphology of crept A) SiC-5YAG and B) SiC-15YAG, showing evidence of redistribution of the secondary phase. The arrows indicate the compression axis.

Figure 5. Low-magnification SEM micrographs of SiC-5YAG after creep, showing the severe cavitation A) close to the center of the sample, B) between the center and surface of the sample and, C) close to the surface of the sample. Cavitation was observed to increase in importance as one approaches the surface of the sample. Also observed is the elongation of the cavities in a plane perpendicular to the compression axis, represented by the arrows.

Figure 6. Low-magnification SEM micrographs of SiC-15YAG after creep, showing the severe cavitation A) close to the center of the sample, B) between the center and surface of the sample and, C) close to the surface of the sample. Cavitation was observed to increase in importance as one approaches the surface of the sample. Also observed is the elongation of the cavities in a plane perpendicular to the compression axis, represented by the arrows.

Figure 7. Low-magnification SEM micrographs close to the surface of A) SiC-5YAG and B) SiC-15YAG after heat-treatment at 1625 ºC under Ar atmosphere in the absence of applied load.

Figure 8. EDX spectra (0-3 keV) from SEM analysis for A) SiC-5YAG and B) SiC-5YAG before and after the creep tests. The peak at 0.68 keV is attributed to F, which is due to the plasma etching.

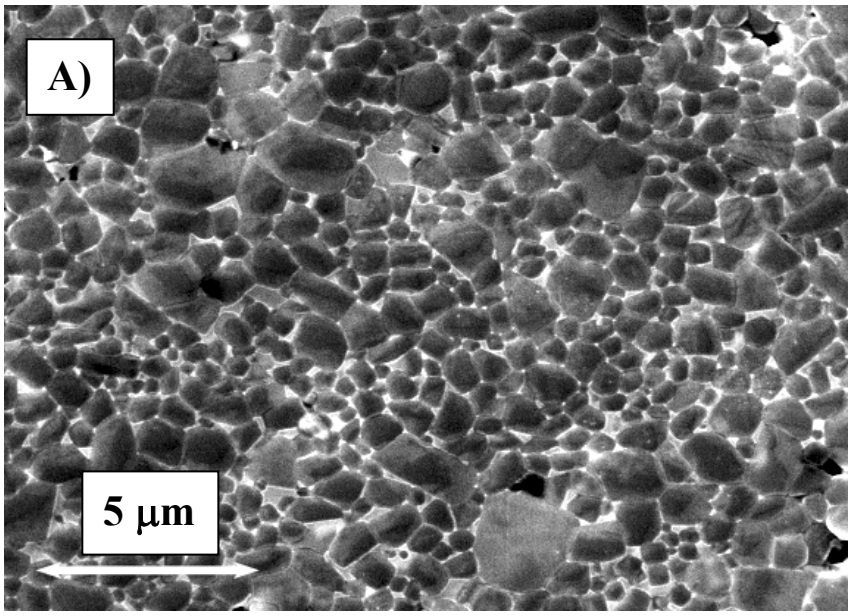

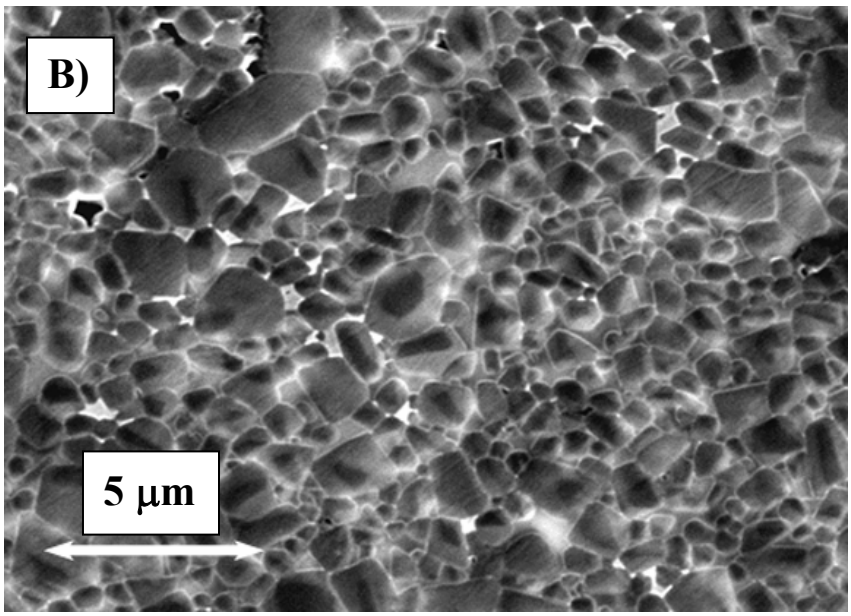

Figure 1. SEM micrographs of as-processed A) SiC-5YAG and B) SiC-15YAG showing the grain morphology and phases present.

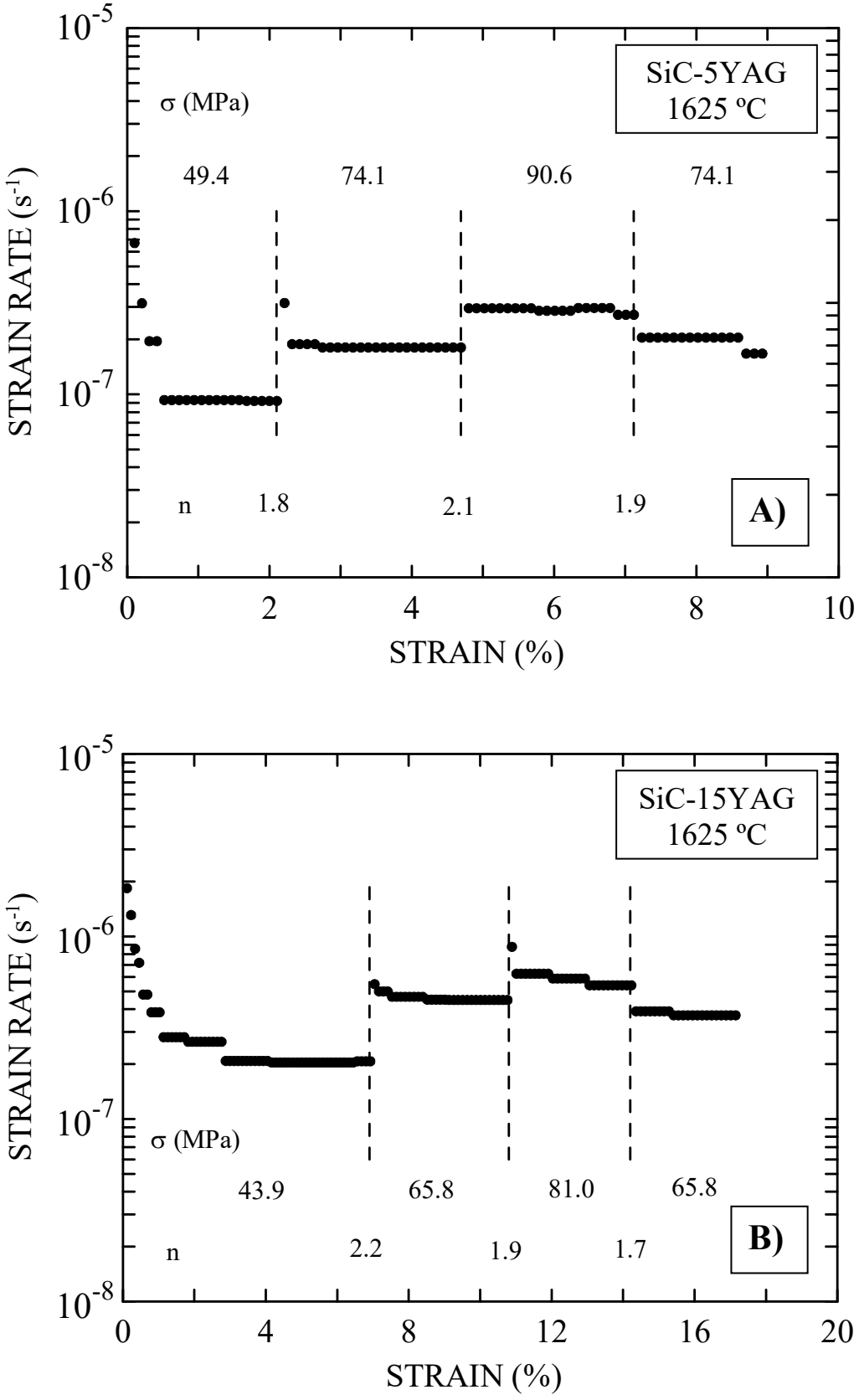

Figure 2. Creep curves at 1625 ºC for A) SiC-5YAG (stresses between 49 and 91 MPa up to about 10% of strain) and B) SiC-15YAG (stresses between 43 and 81 MPa up to about 16% of strain). The values of the stress exponent obtained from each stress change are shown.

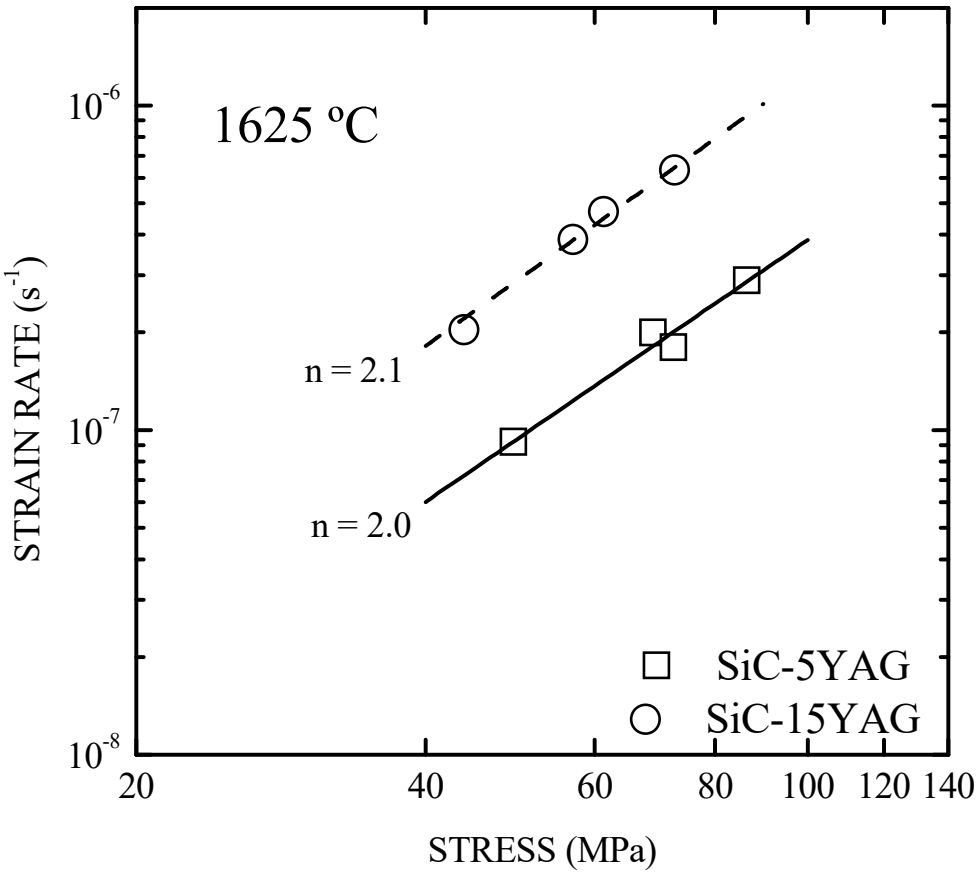

Figure 3. Strain rate versus stress logarithmic plot for SiC-5YAG and SiC-15YAG under the experimental conditions used in this study. The average stress exponent obtained by lineal fit is shown for each case.

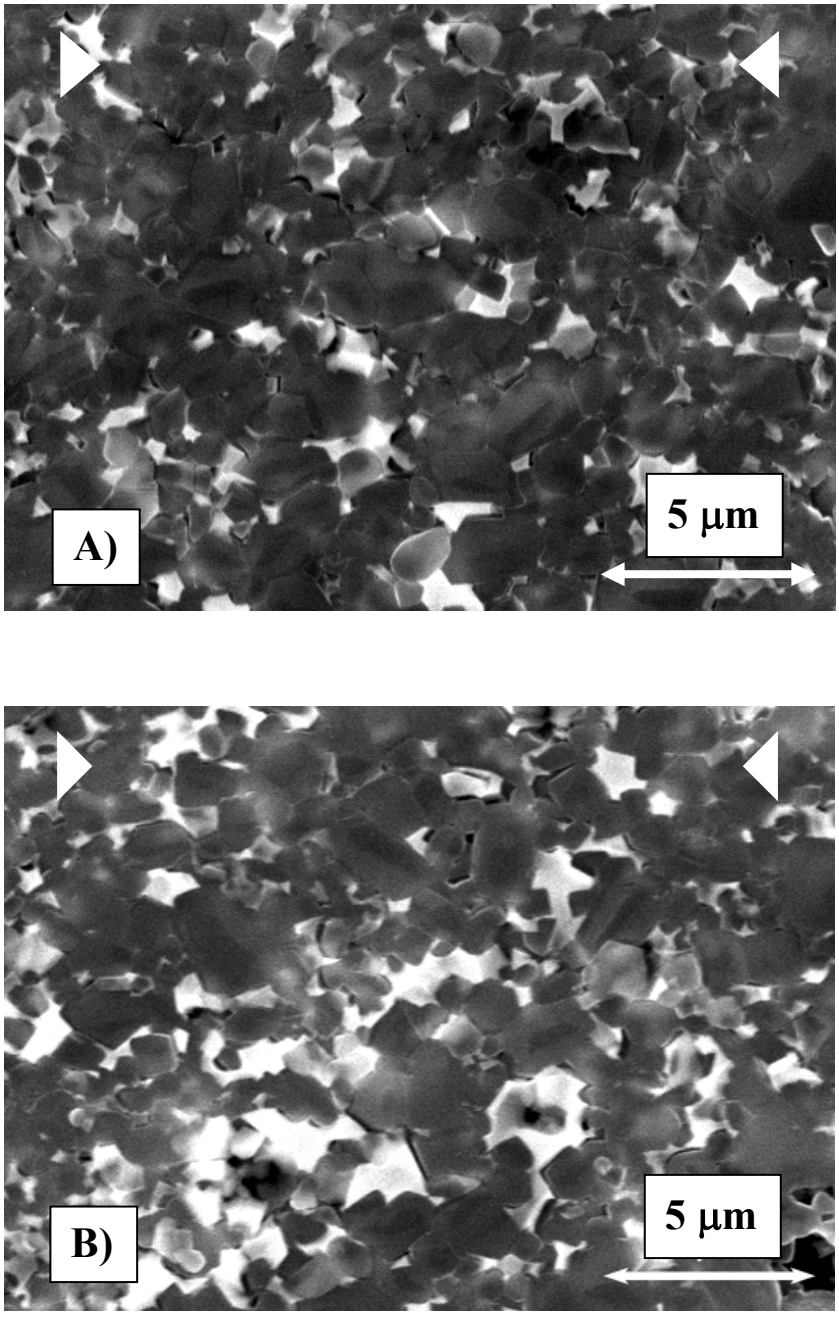

Figure 4: Grain morphology of crept A) SiC-5YAG and B) SiC-15YAG, showing evidence of redistribution of the secondary phase. The arrows indicate the compression axis.

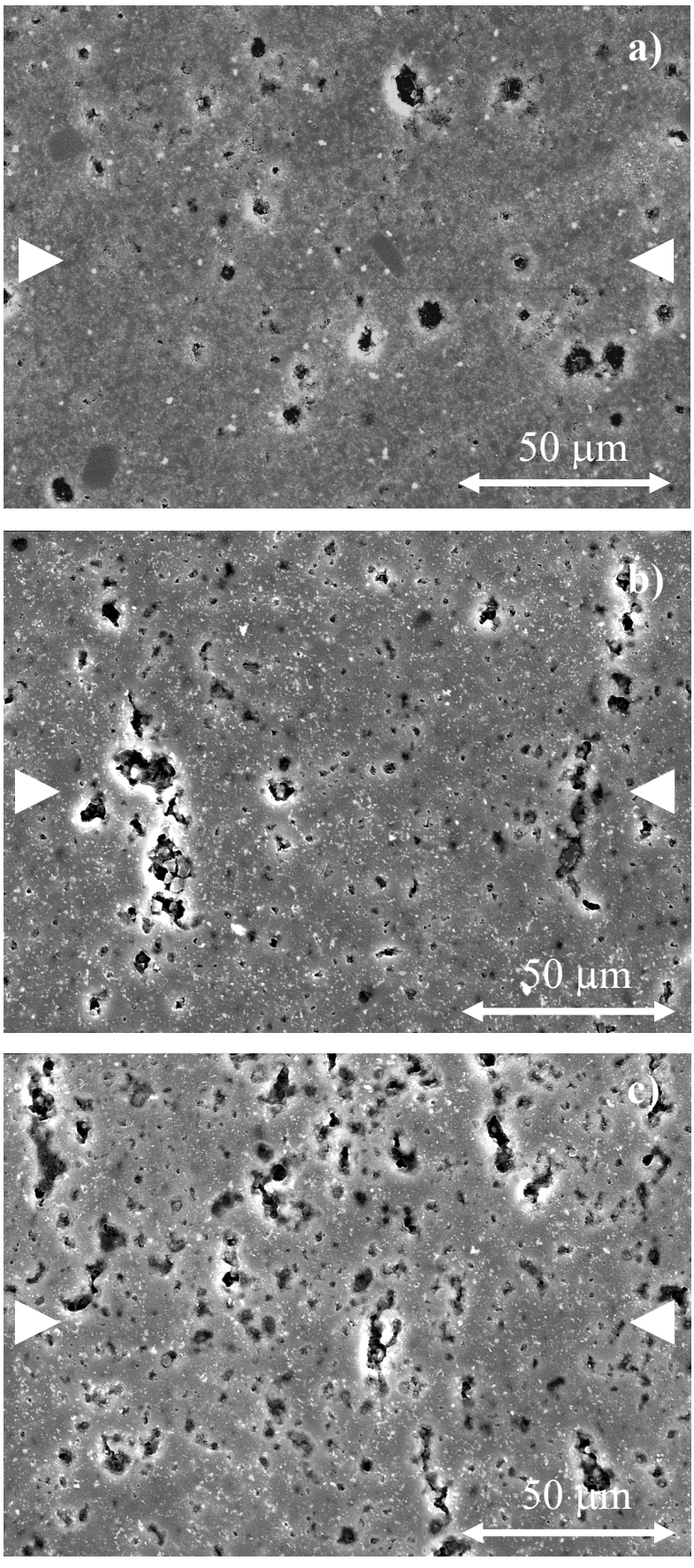

Figure 5. Low-magnification SEM micrographs of SiC-5YAG after creep, showing the severe cavitation A) close to the center of the sample, B) between the center and surface of the sample and, C) close to the surface of the sample. Cavitation was observed to

increase in importance as one approaches the surface of the sample. Also observed is the elongation of the cavities in a plane perpendicular to the compression axis, represented by the arrows.

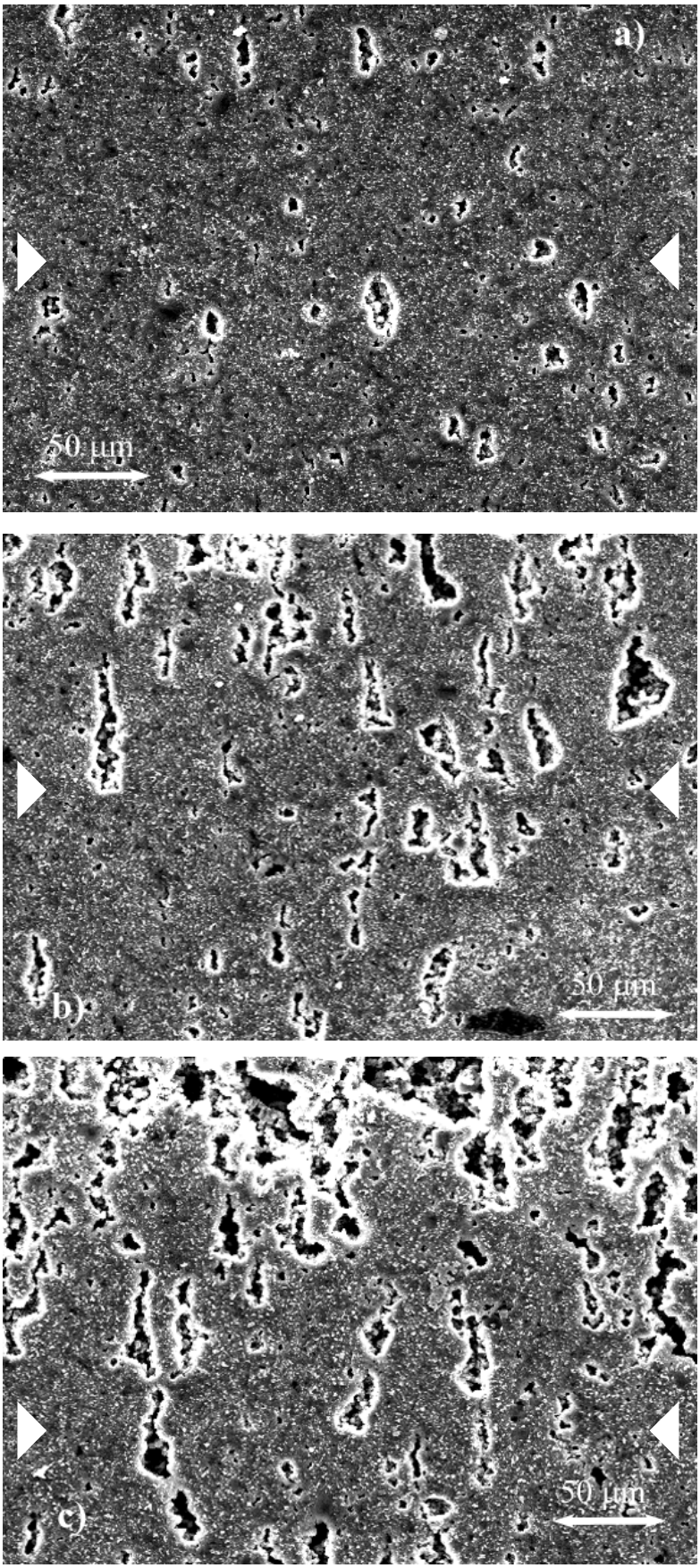

Figure 6. Low-magnification SEM micrographs of SiC-15YAG after creep, showing the severe cavitation A) close to the center of the sample, B) between the center and surface of the sample and, C) close to the surface of the sample. Cavitation was observed to

increase in importance as one approaches the surface of the sample. Also observed is the elongation of the cavities in a plane perpendicular to the compression axis, represented by the arrows.

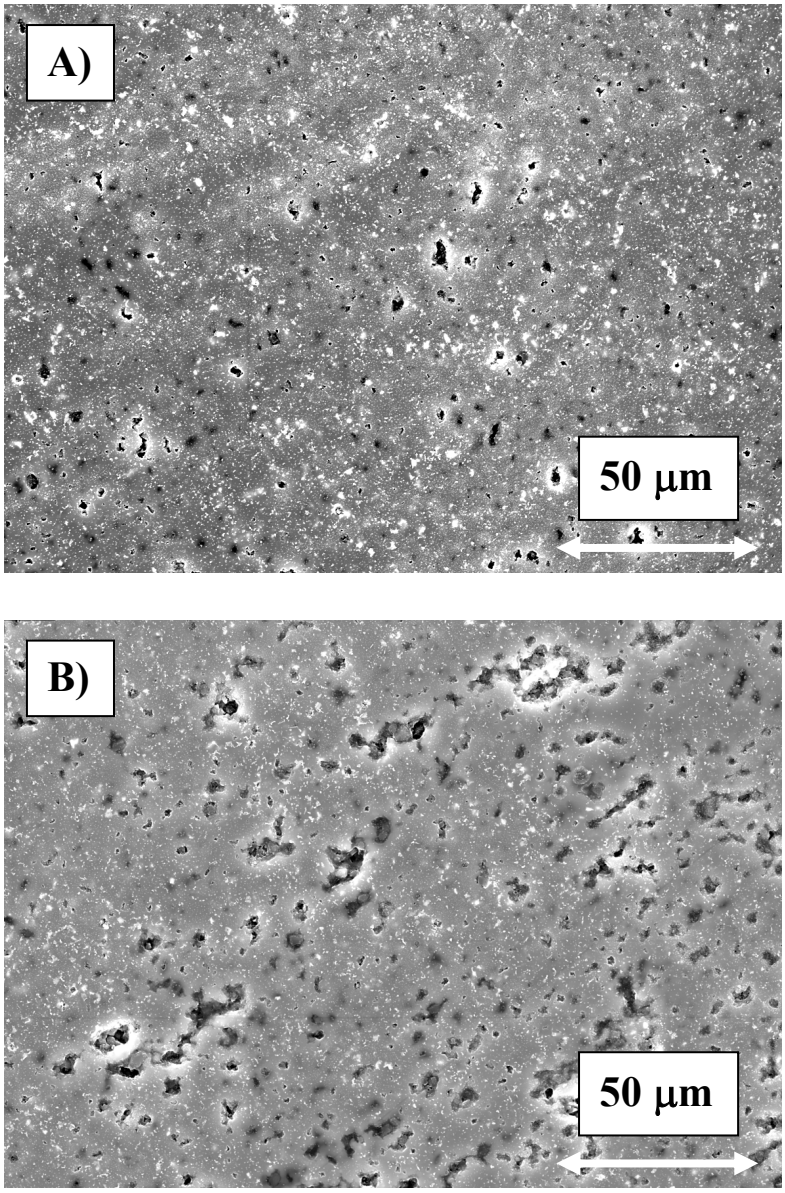

Figure 7. Low-magnification SEM micrographs close to the surface of A) SiC-5YAG and B) SiC-15YAG after heat-treatment at 1625 ºC under Ar atmosphere in the absence of applied load.

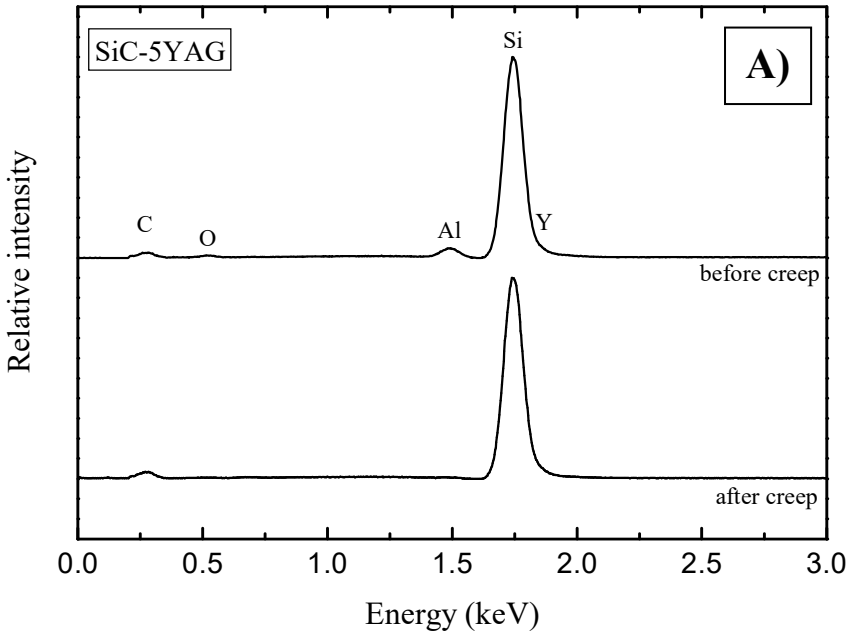

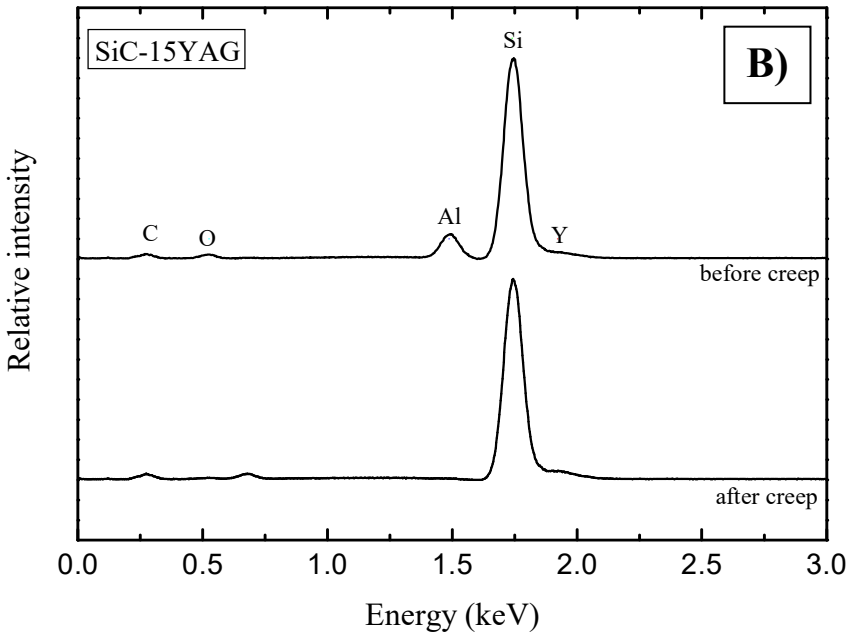

Figure 8. EDX spectra (0-3 keV) from SEM analysis for A) SiC-5YAG and B) SiC-15YAG before and after the creep tests. The peak at 0.68 keV is attributed to F, which is due to the plasma etching.

Table 1. Characteristics of the two materials prepared in this study.

Material*	Powder batch composition (wt. %)			Grain size d (μm)	Form factor (F)	Elastic modulus E (GPa)	Hardness H_V (GPa)	Toughness K_{IC} (MPa·m$^{1/2}$)
	α-SiC	Al_2O_3	Y_2O_3					
SiC-5YAG	95	2.147	2.853	0.7 ± 0.3	0.95 ± 0.1	410 ± 3	24.0 ± 0.6	2.4 ± 0.1
SiC-15YAG	85	6.441	8.559	0.8 ± 0.3	1.0 ± 0.3	375 ± 5	19.4 ± 0.3	3.1 ± 0.1

* SiC-xYAG, where x refers to YAG proportion in weight %.